The Microwave Spectrum of the Two-Top Molecule 2-Acetyl-3-methylthiophene

Christina Dindić, Ha Vinh Lam Nguyen

The Microwave Spectrum of the Two-Top Molecule 2-Acetyl-3-methylthiophene

Christina Dindić[a] and Ha Vinh Lam Nguyen[b,c*]

[a] *Institute of Physical Chemistry, RWTH Aachen University, Landoltweg 2, D-52074 Aachen, Germany*

[b] *Univ Paris Est Creteil and Université de Paris, CNRS, LISA, F-94010 Créteil, France*

[c] *Institut Universitaire de France (IUF), F-75231 Paris cedex 05, France*

***** Corresponding author: lam.nguyen@lisa.ipsl.fr

Abstract

The microwave spectrum of 2-acetyl-3-methylthiophene (2A3MT) was recorded in the frequency range from 2 to 26.5 GHz using a molecular jet Fourier transform microwave spectrometer and could be fully assigned to the *anti*-conformer of the molecule, while the *syn*-conformer was not observable. Torsional splittings of all rotational transitions in quintets due to internal rotations of the acetyl methyl and the ring methyl groups were resolved and analyzed, yielding barriers to internal rotation of 306.184(46) cm^{-1} and 321.813(64) cm^{-1}, respectively. The rotational and centrifugal distortion constants were determined with high accuracy, and the experimental values are compared to those derived from quantum chemical calculations. The experimentally determined inertial defect supports the conclusion that *anti*-2A3MT is planar, even though a number of MP2 calculations predicted the contrary.

Graphical abstract

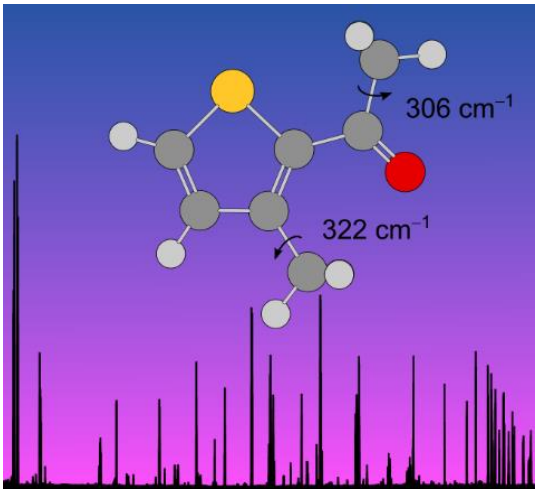

Introduction

Large Amplitude Motion (LAM) has been a classic topic in microwave spectroscopy along its whole history over the last several decades.[1-3] Among them, the most extensively studied LAM is probably the internal rotation of methyl groups. The spectral feature includes torsional fine structures and is significantly more complicated than that of a simple rigid-rotor molecule.

Due to internal rotation, energy levels of each vibrational state split into an A level and an E level in the case of one-top molecules, as illustrated in Figure 1. The splittings visible in the rotational spectrum, called the A-E splittings, are in dependence of the potential barrier hindering the internal rotation. For an infinite barrier height, the torsion of a methyl group could be described as three harmonic oscillators. Each vibrational level is three-fold degenerated, and therefore, no torsional splitting is observed in the spectrum.[4] The molecule can be considered as a rigid rotor, with thousands of molecules previously studied using high resolution rotational spectroscopy, stretching several important subjects from fundamental interest,[5-7] structure determination,[8-10] astrophysics,[11-13] biomolecules,[14-16] chirality[17-19] to microsolvation[20-22] and complexes.[23,24] A barrier of zero, on the other hand, describes a free internal rotor where all energy levels except the first one are two-fold degenerated, as shown, e.g., for the methyl group in CH_3–C≡C–CF_3.[25] Cases between a rigid rotor and a free internal rotor are also often investigated, where A-E splittings are visible in the spectrum and can be used to gain insights regarding the structures and dynamics of the molecule. Molecules featuring one methyl internal rotation, such as 3-methylphenylacetylene,[26] methyl cyanoacetate,[27] 3-methylfuran,[28] 2-butynoic acid,[29] methyl vinyl ketone,[30] and methacrylic acid,[31] have already been extensively studied. However, the number of investigations decreases significantly if the number of internal rotors increases. While dozens of two-top molecules studied by high resolution spectroscopy can still be found in the literature,[32-34] only a handful of three-top molecules have been reported[35-37] and only one four-top molecule is found in an on-going study.[1,38] Such molecules with multiple methyl internal rotors exhibit complicated spectral features, depending on the number of rotors and their interactions. For example, in a molecule featuring two methyl groups, the fine structure consists of quartets in the case of two equivalent methyl tops, or quintets for two inequivalent ones (see Figure 1).[39]

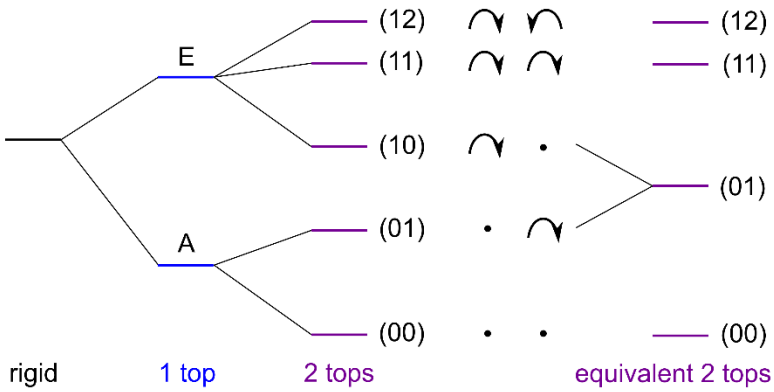

Figure 1: Schematic energy level diagram illustrating the splittings caused by internal rotation for (i) a rigid rotor (no torsional splitting), (ii) a molecule containing one methyl rotor (splitting into an A and an E species), and (iii) a molecule containing two inequivalent methyl rotors (splitting into five torsional species). A dot symbolizes the $\sigma = 0$ state, a clockwise arrow the $\sigma = 1$ and an anti-clockwise arrow the $\sigma = -1$ state.[39]

LAM containing molecules with conjugated π-double bonds are of special interest as electronic effects can be transferred across a longer range, often enabling interactions between two internal rotors. Examples are investigations on a number of benzene derivatives featuring two methyl internal rotations such as three isomers of dimethylanisole,[40-42] three isomers of dimethylbenzaldehyde,[43] *o*- and *m*-xylene,[44,45] two isomers of dimethylfluorobenzene,[46,47] 4-methylacetophenone,[48] or some five-membered aromatic rings like the 2,5-isomers of dimethylthiophene,[49] dimethylfuran,[50] and dimethylpyrrole[51] or 2-acetyl-5-methylfuran[52] and 4,5-dimethylthiazole.[53] In these studies, it was clearly proven that steric hindrance arising from a neighboring substituent increases the torsional barrier of a methyl group attached to the aromatic ring, but also that electrostatic effects can be transferred across the π-conjugated system and influence the methyl torsion. While it is easy to expect whether steric effects may occur, the exact nature of electrostatic interactions has not been fully explored yet, mainly due to the very limited number of studies on aromatic heterocycles containing more than one methyl internal rotation. Therefore, we aim at a systematic investigation on such molecules with several methyl rotors for a better understanding of these long-range effects. In the present study, the LAMs of 2-acetyl-3-methylthiophene (2A3MT), illustrated in Figure 2, will be probed by a combination of microwave spectroscopy and quantum chemistry. 2A3MT features a methyl rotor attached at the third position of the thiophene ring and an acetyl group at the neighboring second position, which also contains a methyl rotor. The π-conjugated system of thiophene is extended by the carbonyl group, therefore connecting the two methyl torsions. Barrier heights determined for the two tops will

yield valuable data to evaluate the effects of both steric hindrance and electrostatic interactions in thiophene derivatives.

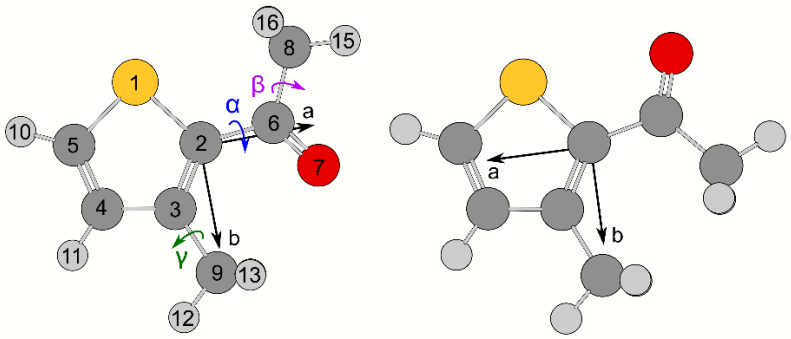

Figure 2: Molecular structures of the two conformers of 2A3MT optimized at the B3LYP-D3BJ/6-311++G(d,p) level of theory in their principal axes of inertia. Atom numbering and the dihedral angles α = ∠(S1–C2–C6=O7), β = ∠(C2–C6–C8–H15), and γ = ∠(C2–C3–C9–H12) are defined for *anti*-2A3MT. The sulfur atom is marked in yellow, oxygen atom in red, carbon atoms are in dark grey, and hydrogen atoms in light grey. H14 lies behind H13, H17 behind H16.

2. Quantum chemical calculations

2.1. Conformational analysis

The planarity of the thiophene ring has been established in the literature.[9,54] Therefore, the conformational landscape of 2A3MT is only influenced by the orientation of the two substituents attached to the ring. As the rotation of the methyl group about the C3–C9 bond does not create new conformers, only the acetyl group has to be rotated for a conformational search. Based on investigations on similar molecules containing an acetyl group and an aromatic ring such as 2-acetylfuran,[55] 2-thiophenecarboxaldehyde,[56] and 2-acetyl-5-methylfuran,[52] it is reasonable to expect two conformers, either with the oxygen atom in an *anti*- or a *syn*-position in relation to the sulfur atom. For the conformational analysis, the dihedral angle α = ∠(S1–C2–C6=O7) (for atom numbering see Figure 2) was varied in steps of 10° while all other geometry parameters were optimized at the MP2/6-311++G(d,p) level of theory using the *Gaussian 16* program package.[57] This level was chosen, because it predicted rotational constants close to the experimental values for many classes of molecules to guide the spectral assignment,[58-61] and is therefore the level most frequently used in our previous investigations.[62-64] The calculated energies were parameterized using a Fourier expansion

with the corresponding coefficients given in Table S-1 of the Supplementary Material. With these Fourier coefficients, the potential energy curve shown in Figure 3 could be drawn. Surprisingly, it does not exhibit the expected two minima at 0° and 180°, corresponding to the typical *syn*- and *anti*-conformers, respectively, but a very wide valley around 0° and a flat double minimum around 180°. To explore these areas, α was varied in steps of 1° between −10° and 10° as well as 160° and 200° as shown in Figure 4. We found a very shallow double minimum in the area between −5° and 5°, with the minima lying at ±1.6°, as can be clearly recognized in calculations with a step width of 0.1° shown in the inset of Figure 4. For the area between 160° and 200°, also shown in Figure 4, the two equivalent minima lie at 171° and 189°, but the potential curve is not continuous and exhibits a sudden break between 181° and 182°. According to these calculations, both the *anti*- and the *syn*-conformer of 2A3MT exist as two equivalent, non-planar forms, where the acetyl moiety is tilted by 9.0° and 1.6° out of the thiophene plane, respectively. However, since (i) the structure of a similar molecule, 2-acetylfuran, was experimentally determined to be planar by isotopic substitutions,[55] (ii) our investigation on 2-propionylthiophene showed that the planarity of a thiophene derivative with a carbonyl group containing substituent depends strongly on the level of theory in use,[65] and (iii) similar observations having been made for nitroxoline,[66] another molecule containing conjugated π-double bonds, we repeated the calculations using the B3LYP-D3BJ method. The potential energy curves, also illustrated in Figures 3 and 4, exhibit the expected course with only two minima, showing that both conformers of 2A3MT are planar. Subsequently, full structure optimizations were performed at both levels of theory, with additional frequency calculations confirming the two obtained conformers to be stable. The calculated rotational constants, dipole moment components, dihedral angles, and energy differences are summarized in Table 1; the atomic coordinates are given in Table S-2 of the Supplementary Material. The *anti*-conformer is predicted to be much more stable than the *syn* one.

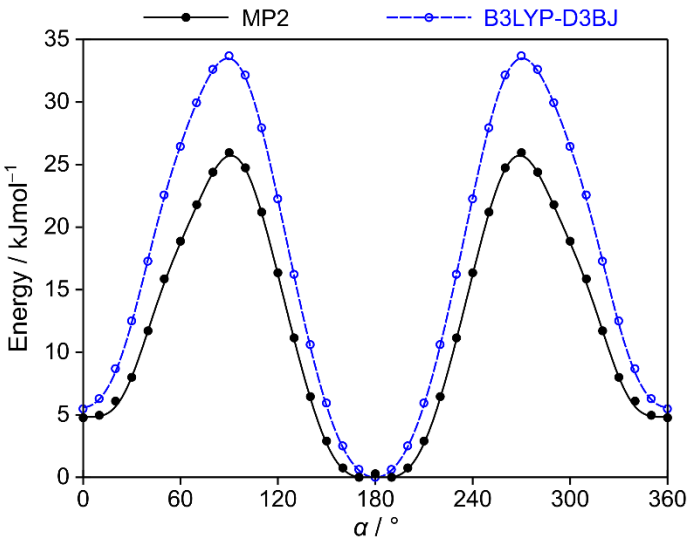

Figure 3: The potential energy curves of 2A3MT obtained by rotating the acetyl group about the C2–C6 bond (for atom numbering see Figure 2). Calculations were performed at the MP2/6-311++G(d,p) and B3LPY-D3BJ/6-311++G(d,p) levels of theory by varying the dihedral angle *α* in a grid of 10°. The relative energies are given in respect to the lowest energy conformation with E_{MP2} = –743.5343631 Hartree and $E_{B3LYP\text{-}D3BJ}$ = –745.1266413 Hartree.

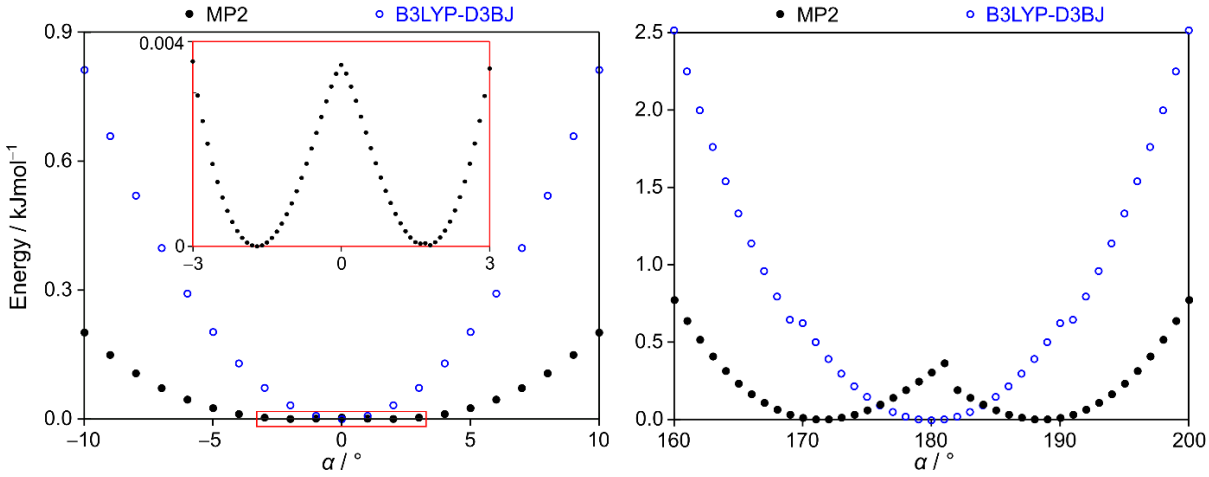

Figure 4: **Left hand side:** The portion between –10° and 10° of the potential energy curves of 2A3MT given in Figure 3 where the dihedral angle *α* was varied in a grid of 1°. The relative energies are given in respect to the lowest energy points with E_{MP2} = –743.5325478 Hartree and $E_{B3LYP\text{-}D3BJ}$ = –745.1245546 Hartree. The inset shows the region between –3° and 3° in a step width of 0.1° calculated at the MP2/6-311++G(d,p) level of theory with the lowest energy point at $E_{MP2,inset}$ = –743.5325481 Hartree. **Right hand side:** The portion between 160° and 200° where the dihedral angle *α* was varied in a grid of 1°. The relative energies are given in respect to the lowest energy points with E_{MP2} = –743.5343669 Hartree and $E_{B3LYP\text{-}D3BJ}$ = –745.1266413 Hartree.

Table 1: Rotational constants (in MHz), dipole moments (in D), dihedral angles (in degrees), and relative energies (in kJ·mol^{-1}) for the two conformers of 2A3MT calculated with the MP2 and B3LYP-D3BJ methods and the 6-311++G(d,p) basis set.

Par.	*MP2*		*B3LYP-D3BJ*	
	anti	***syn***	***anti***	***syn***
A_e	1991.5	1990.2	1990.5	1994.8
B_e	1406.2	1397.8	1407.0	1395.1
C_e	836.9	829.7	832.7	829.4
$\lvert\mu_a\rvert$	2.11	1.60	2.54	1.55
$\lvert\mu_b\rvert$	1.40	4.49	1.24	3.94
$\lvert\mu_c\rvert$	0.43	0.08	0.00	0.00
α	171.47	−1.68	180.00	0.01
β	173.80	179.08	−179.99	179.99
γ	−173.21	177.91	−179.99	179.99
ΔE^a	0.0	4.6	0.0	6.9

[a] Energy differences including zero-point corrections relative to the most stable conformer *anti*-2A3MT with E_{MP2} = −743.402494 Hartree and $E_{B3LYP\text{-}D3BJ}$ = −744.992915 Hartree.

2.2. Basis set variations

Due to the discrepancies between the MP2 and B3LYP methods used for the structure optimizations, as well as a benchmarking effort attempting to find a level of theory which allows for a cost-efficient yet reasonably accurate prediction of rotational constants to ease the assignment of microwave spectra of similar molecules, geometry optimizations were repeated using different methods and basis sets. In addition to the MP2[67] and B3LYP[68,69] methods, the *ab initio* CCSD[70] method as well as other density functional theory M06-2X[71] and ωB97X-D[72] methods were employed. Furthermore, the B3LYP functional was used both with Grimme's dispersion correction including Becke-Johnson damping (D3BJ)[73] and without (D3),[74] but also in combination with the Coulomb-attenuating method (CAM-B3LYP).[75] These methods were combined with a variety of basis sets, such as Pople's basis sets[76] (6-31G or 6-311G) without or with diffuse (+ or ++) functions. Polarization functions like (d,p), (df,dp), (2d,2p), (2df,2pd), (3df,3dp) are included in all cases. Furthermore, polarized valence double- (cc-pVDZ) and triple-zeta (cc-pVTZ) Dunning's basis sets were also utilized,[77] without or with diffuse functions included in the augmented basis sets known as aug-cc-pVDZ and aug-cc-pVTZ.[78]

All calculations were exclusively performed for *anti*-2A3MT, as only this conformer was eventually observed in the microwave spectrum. The results are given in Table S-3 in the Supplementary Material and will be discussed in comparison to the experimental values in the section 4.

2.3. Methyl internal rotations

The acetyl methyl and the ring methyl group are both internal rotors. The barriers hindering the internal rotation were calculated by varying the dihedral angles β = ∠(C2–C6–C8–H15) and γ = ∠(C2–C3–C9–H12) in 10° steps. All other geometry parameters were optimized at the MP2 and B3LYP-D3BJ/6-311++G(d,p) levels of theory because (i) it was unclear at this point whether the geometry of 2A3MT is planar as predicted with the B3LYP-D3BJ method or non-planar as given by the MP2 method, and (ii) in some previous studies, MP2 calculations often overestimate and B3LYP ones underestimate values of torsional barriers.[49,65,79] Using both methods thus enables a better estimation. The resulting potential energy curves for *anti*-2A3MT are shown in Figure 5, those of *syn*-2A3MT in Figure S-1 in the Supplementary Material. Coefficients of the Fourier expansion used to plot the potential curves can be found in Table S-4. Again, further discussions will only focus on *anti*-2A3MT.

The values predicted with the MP2 method are larger than those of the B3LYP-D3BJ calculations as expected. For the acetyl methyl group of *anti*-2A3MT, we found calculated barriers of 316.1 cm^{-1} (MP2) and 182.7 cm^{-1} (B3LYP-D3BJ). The respective values for the ring methyl group are 424.8 cm^{-1} and 263.4 cm^{-1}. Further discrepancies between the two methods are the different V_6 contributions, resulting in a double minimum potential for the MP2 curves but a typical three-fold potential for the B3LYP-D3BJ curves, as can be clearly recognized in a portion of the curves between 40° and 80° recalculated in 2° steps (see the inset of Figure 5). This observation is likely due to the couplings between the two methyl torsions, which is more significant in MP2 calculations, as shown in the lower trace of Figure 5. The rotation of one methyl group induces an oscillation of up to 15° of the other methyl group in calculations with the MP2 method, whereas almost no oscillation is observed in B3LYP-D3BJ calculations. Due to the rearrangement of the acetyl group upon methyl torsions, the MP2 potential curve shows a sudden discontinuation at 66°, the B3LYP-D3BJ exhibits two at 48° and 70°.

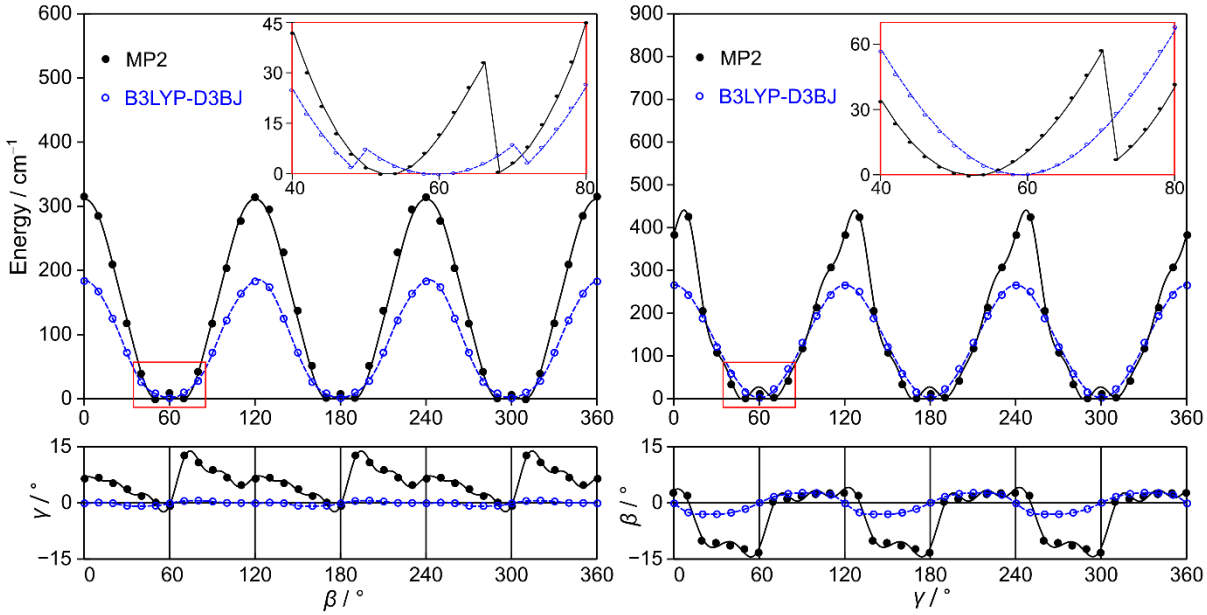

Figure 5: Left hand side: The potential energy curves of *anti*-2A3MT obtained by rotating the acetyl methyl group about the C6–C8 bond by varying the dihedral angle β in steps of 10°. The calculations were performed using the 6-311++G(d,p) basis set with either the MP2 or the B3LYP-D3BJ method. The energies are given relative to the lowest energy with E_{MP2} = –743.5343577 Hartree and $E_{B3LYP\text{-}D3BJ}$ = –745.1266412 Hartree. The calculated barrier heights are 316.1 cm^{-1} (MP2) and 182.7 cm^{-1} (B3LYP-D3BJ). The MP2 potential exhibits a flat double minimum at $\beta \approx$ 60°, 180°, and 300°. The inset shows the portion between 40° and 80° obtained by varying β in steps of 2°. The energy data points are connected by a non-parameterized curve, which is only present for a better tracing. The lower trace depicts the oscillation of the ring methyl group upon the rotation of the acetyl methyl group. The deviations of the dihedral angle γ are given relative to the values of –173.21° (MP2) and –179.99° (B3LYP-D3BJ) of the fully optimized geometries. **Right hand side:** The potential energy curves of *anti*-2A3MT obtained by rotating the ring methyl group about the C3–C9 bond by varying the dihedral angle γ in steps of 10°. The energies are given relative to the lowest energy with E_{MP2} = –743.5343619 Hartree and $E_{B3LYP\text{-}D3BJ}$ = –745.1266402 Hartree. The calculated barrier heights are 424.8 cm^{-1} (MP2) and 263.4 cm^{-1} (B3LYP-D3BJ). The inset shows the portion between 40° and 80° with γ varied in steps of 2°. The curve connecting the energy points are not parameterized. The MP2 potential curve shows a sudden discontinuation at 69°, while the B3LYP-D3BJ one is continuous. On the lower trace is the oscillation of the acetyl methyl group upon the ring methyl torsion. The deviations of the dihedral angle β are given relative to the values of 173.80° (MP2) and –179.99° (B3LYP-D3BJ) of the fully optimized geometries.

The barriers to internal rotation of the *anti*-conformer were furthermore also predicted at all levels of theory mentioned in section 2.2. The calculated values are listed in Table S3 in the Supplementary Material; a selection of calculations using the 6-311++G(d,p) basis set are given in Table 2. We note at this point that for geometry optimizations, attempts on extensive benchmarking exist, aiming at calculating rotational constants to guide the spectral assignment,[80] but the same is not the case for methyl torsional barriers. The reason might be the challenge in accurate calculations of energies. While 1 kJ·mol^{-1}, corresponding to 84 cm^{-1}, already indicates highly accurate energy calculations, it does not satisfy the experimental requirements, considering that a change of one cm^{-1} in the torsional barrier might lead to a shift of hundreds of MHz of the frequencies in the microwave spectrum.

Table 2: Torsional barriers (in cm^{-1}) of the acetyl methyl and ring methyl group in *anti*-2A3MT calculated with different methods in combination with the 6-311++G(d,p) basis set. The deviations between the experimental values and the calculated ones are given as absolute values (in cm^{-1}) as well as in percent relative to the experimental values in parentheses.

Method	**Acetyl**	**Dev.**	**Ring**	**Dev.**
MP2	316.1	–10 (–3)	424.8	–103 (32)
B3LYP-D3	228.9	77 (25)	306.3	16 (5)
B3LYP-D3BJ	182.7	124 (40)	263.4	58 (18)
CAM-B3LYP-D3BJ	205.5	101 (33)	257.6	64 (20)
M06-2X	288.4	18 (6)	369.8	–48 (–15)
ωB97X-D	248.9	57 (19)	243.9	78 (24)
Experimental	**306.2**		**321.8**	

In order to study the top-top interactions in more detail, we calculated two-dimensional potential energy surfaces (2D-PES) depending on the dihedral angles β and γ. Due to symmetry, only data points in the range from 0° to 120° for both β and γ were necessary. The energy points obtained with the MP2 method once again showed discontinuations due to the rearrangement of the entire acetyl group, similar to the observation illustrated in Figure 5. Therefore, the data points, available in the Supplementary Material (Table S-5), could not be parameterized. Thus, only the 2D-PES calculated with the B3LYP-D3BJ method is shown in Figure 6, where the potential energies were parameterized with a Fourier expansion with the coefficients listed in Table S-6, taking into account the correct symmetry of the methyl groups. The 2D-PES also visualizes that coupling between the two rotors exists, as the minima have oblate rather than circular forms, which would be the case if there were no top-top interaction.

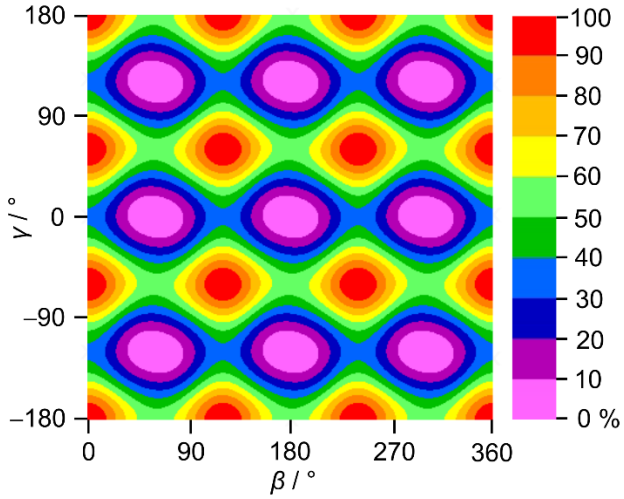

Figure 6: Two-dimensional potential energy surface of *anti*-2A3MT calculated at the B3LYP-D3BJ/6-311++G(d,p) level of theory in dependence of the dihedral angles *β* and *γ*, which were varied in a grid of 10° while all other geometry parameters were optimized. The color code gives the relative energy (in percent) on a scale between the minimum E_{min} = −745.124411 Hartree (0%) and the maximum E_{max} = −745.126640 Hartree (100 %).

3. Microwave spectroscopy

As the *anti*-conformer of 2A3MT was predicted to be energetically more stable, we started the assignment with this conformer using the rotational constants calculated at the MP2/6-311++G(d,p) level of theory given in Table 1. These values were used to predict a rigid-rotor spectrum with the program *XIAM*[81] without taking the effects of internal rotation into account. From the calculated dipole moments, *a*- and *b*-type transitions were expected to be very strong while *c*-type transitions should not be visible.

The initial assignment was successful without any problems as the four most intense transitions of the entire survey spectrum ($5_{05} \leftarrow 4_{14}$, $5_{15} \leftarrow 4_{14}$, $5_{05} \leftarrow 4_{04}$, $5_{15} \leftarrow 4_{04}$) were less than 2 MHz off from their predicted frequencies. After a satisfactory rigid rotor fit for *anti*-2A3MT had been achieved, the fit was expanded to include the internal rotation effects. Since the two methyl rotors are inequivalent, each transition of 2A3MT splits into five torsional components ($\sigma_1\sigma_2$) = (00), (01), (10), (11), and (12) as shown in Figures 1 and 7, where σ_1 and σ_2[39,41] refer to the acetyl methyl and the ring methyl group, respectively. In a first step, we started with two separate one-top fits, consisting of only the (00) and (01) or (10) torsional species, and neglected the (11) and (12) species representing top-top interactions. Since quantum chemical calculations predicted a higher barrier to internal rotation for the ring methyl group, we assumed splittings between the (00) and (10) species to be smaller than the (00)-(01) ones. However, in the experimental spectrum this difference was not as significant as expected.

Furthermore, the (11)-(12) splittings are often at the resolution limit and not distinguishable. In the high resolution measurement of the *a*-type transition $5_{15} \leftarrow 4_{14}$ shown in Figure 7, the separations between the (00) and (01), (01) and (10), (10) and (11), and (11) and (12) species are 114.9 kHz, 31.5 kHz, 112.5 kHz, and 4.5 kHz, respectively. Due to the small splittings, it was difficult at the beginning to assign the torsional species correctly, including the (00) species which should follow a semi-rigid rotor Hamiltonian model. In order to identify the correct torsional species we employed two approaches. Firstly, we focused on rotational transitions with higher K_a quantum numbers, because the fine splittings are larger and it is thus easier to distinguish a torsional species from the other ones. Secondly, the program *SFLAMS* (Separately Fitting of Large Amplitude Motion Species)[82] was employed to fit the (00), (01), and (10) species separately to check the correctness of the assignment. Eventually, two one-top fits with experimental accuracy could be achieved with the program *XIAM* and finally combined in a two-top fit consisting of the (00), (01), and (10) species. The remaining (11) and (12) species could then be predicted, measured, and assigned straightforwardly. The *XIAM* global fit shown in Table 3 incorporates 751 lines in total. The number of lines is nearly evenly distributed between the five species, with a slightly larger number for the (00), (01), and (10) species due to their higher spin statistical weight.[41] The assigned transitions are listed in Table S-7 in the Supplementary Material. The separate fits with the program *SFLAMS* are given in Table S-8. The rotational constant F_0, describing the moment of inertia of the methyl internal rotor, could not be fitted and was fixed to 158 GHz, a value often found for methyl groups. The average line width at half height is 21 kHz, corresponding to an estimated measurement accuracy of 2.1 kHz, which is $1/10^{th}$ of the average line width.

After the assignment of the *anti*-conformer, some very weak lines remained in the spectrum. They most likely belong to either the *syn*-conformer or isotopologues of *anti*-2A3MT, but further assignment was not possible due to the small number of lines and their low intensity.

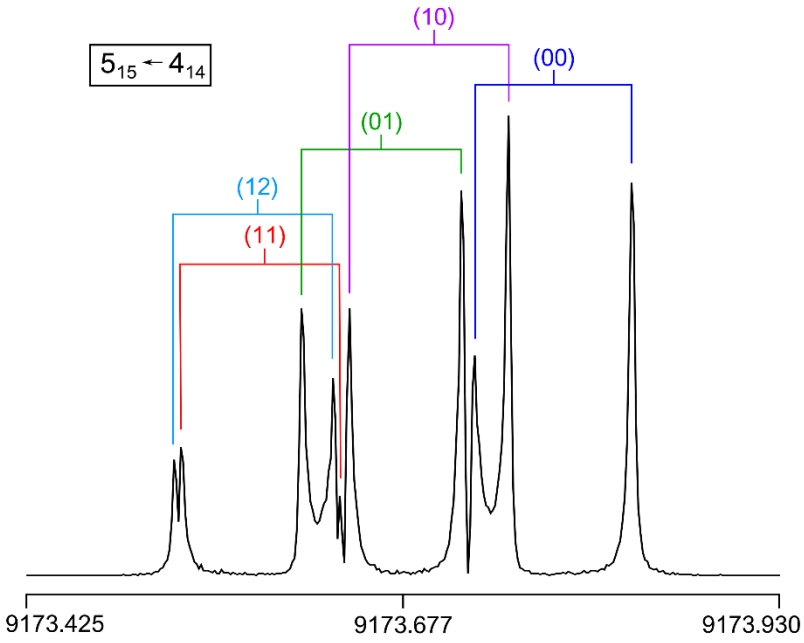

Figure 7: A typical high resolution measurement of the *a*-type rotational transition $5_{15} \leftarrow 4_{14}$ with its five torsional species (00), (10), (01), (11), and (12). The frequency is given in MHz. The brackets indicate Doppler pairs. The spectrum was recorded at 9173.79 MHz, and 200 free induction decays were co-added.

Table 3: Experimental spectroscopic parameters of *anti*-2A3MT obtained with the program *XIAM* compared to the predicted values.

Par.	Unit	*XIAM*[a]	MP2[b]	B3LYP-D3BJ[b]
A_0	MHz	1997.975481(81)	1977.436	1977.164
B_0	MHz	1411.966335(69)	1398.860	1395.869
C_0	MHz	836.288600(23)	826.460	827.099
Δ_J	kHz	0.04798(24)	0.0546	0.0465
Δ_{JK}	kHz	0.0444(12)	0.0255	0.0414
Δ_K	kHz	0.0412(39)	0.0480	0.0383
δ_J	kHz	0.01801(12)	0.0197	0.0176
δ_K	kHz	0.07556(59)	0.1451	0.0941
$V_{3,1}$	cm^{-1}	306.184(46)	316.1	182.7
$D_{p_i^2 J,1}$	kHz	55.3(11)		
$D_{p_i^2 K,1}$	kHz	–120.6(21)		
$D_{p_i^2 -,1}$	kHz	32.7(35)		
$\angle(i_1,a)$	deg	61.304(20)	65.5	65.1
$\angle(i_1,b)$	deg	28.695(20)	26.3	24.9
$\angle(i_1,c)$	deg	90.0[c]	81.0	90.0
$V_{3,2}$	cm^{-1}	321.813(64)	425.8	263.4

$D_{p_i^2 J,2}$	kHz	75.0(12)		
$D_{p_i^2 K,2}$	kHz	55.2(22)		
$D_{p_i^2 -,2}$	kHz	37.6(13)		
∠(i_2,*a*)	deg	72.128(16)	68.5	69.3
∠(i_2,*b*)	deg	17.872(16)	21.9	20.7
∠(i_2,*c*)	deg	90.0[c]	88.1	90.0
N[d]		751		
σ[e]	kHz	2.2		

[a] All parameters refer to the principal axis system. Watson's A reduction and I^r representation were used. [b] Calculated with the 6-311++G(d,p) basis set. Ground state rotational constants and centrifugal distortion constants obtained from anharmonic frequency calculations are given. The centrifugal distortion constants were transformed from III^r to I^r representation using Eq. (6) of Ref. [83]. [c] Fixed due to symmetry. [d] Number of transitions. [e] Standard deviation of the fit.

4. Discussion

For 2A3MT only the *anti*-conformer was visible in the spectrum, confirming the predicted higher energetic stability of the *anti*-orientation over the *syn* one. In other thiophene derivatives like 2-thiophenecarboxaldehyde[56] and 2-propionylthiophene,[65] the *syn*-conformer is more stable than the *anti*-form. The conformational stability was explained by dipole-dipole interactions between the positively charged sulfur atom and the negatively charged oxygen atom of the acetyl group, which still holds true in the case of 2A3MT. NBO calculations[84] performed using the *Gaussian 16* program package[57] yield the charge distribution of 2A3MT depicted in Figure 8, showing that the negative partial charge on the carbon atom of the acetyl methyl group is larger than that of the oxygen atom, which stabilizes the *anti*-form over the *syn*-form. Furthermore, the methyl group at the third position of the ring induces steric interactions between the two methyl groups in the *syn*-form where the positive partial charged hydrogen atoms are closest to each other. In constrast, in the *anti*-conformer the negative partial charged oxygen atom of the acetyl group and the positive partial charged hydrogen atoms of the ring methyl group can form a hydrogen bond, thus making the *anti*-orientation significantly more stable, in agreement with the experimental observation. Quantum chemical calculations at all levels of theory also consistently predicted *anti*-2A3MT to be energetically more favorable than the *syn* conformer. Note that the positive partial charge of the sulfur atom causes a negative partial charge on both C(2) and C(5) atoms, while in furfural derivatives, e.g. 2-acetylfuran,[55] they carry a positive partial charge because of the negative partial charge of the oxygen atom in the furan ring.

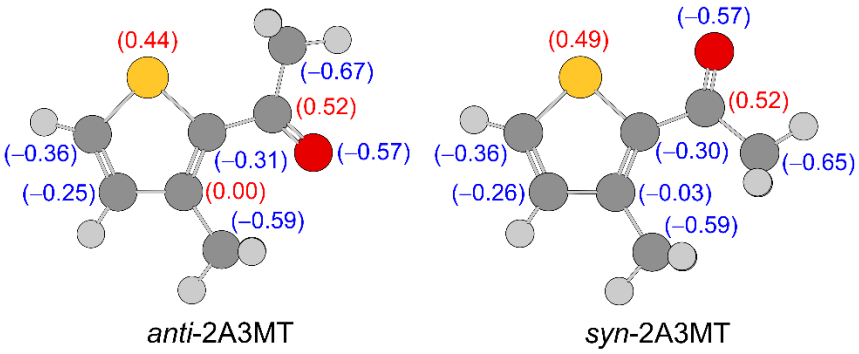

Figure 8: Charge distribution in *anti*- and *syn*-2A3MT obtained from NBO calculations at the B3LYP-D3BJ/6-311++G(d,p) level of theory.

Concerning the molecular geometry, calculations at some levels of theory using the MP2 method predicted a non-planar structure with the acetyl group slightly tilted out of the thiophene plane, while all other calculations predicted a planar structure (see Table S-3 Supplementary Material). It is noticeable that almost all of them include diffuse functions (+ or ++). The only level without diffuse function, MP2/6-311G(df,pd), calculates a much smaller tilt angle of only about 2° of the acetyl group (called angle Θ in Table S-3). A structure determination was not possible because the isotopologue lines of *anti*-2A3MT are not sufficiently intense to be measured. From a comparison of the experimental value of −6.559 uÅ^2 found for the inertial defect of *anti*-2A3MT with the value of −9.288 uÅ^2 calculated using the rotational constants obtained at the MP2/6-311++G(d,p) level, predicting a non-planar structure, and the value of −6.200 uÅ^2 obtained at the B3LYP-D3BJ/6-311++G(d,p) level, predicting a planar structure, we suspect that at least the effective structure is planar. The experimentally determined value is also very close to the inertial defects of other planar molecules with four out-of-plane hydrogen atoms such as the C_s conformer of 2-ethylfuran (Δ_c = −6.483 uÅ^2)[85] and the *cis-trans* conformer of ethylnitrite (Δ_c = −6.422 uÅ^2).[86] We underline at this point that since the isotopologue spectra were not observable, the inertial defect is rather an indication and does not give any conclusive statement on the planarity of 2A3MT.

The *XIAM* fit shown in Table 3 with a total of 751 lines has a standard deviation of 2.2 kHz, which is very close to the experimental accuracy of 2.1 kHz and is therefore quite satisfactory. All rotational and centrifugal distortion constants as well as the internal rotation parameters are determined with high accuracy. A comparison between the experimentally determined rotational constants B_0 deduced from the *XIAM* fit and those calculated at different levels of theory B_e (see Table S-3) is not physically meaningful, as the experimental values correspond to the vibrational ground state while the predicted values belong to the equilibrium structure. Nevertheless, it can be helpful to know which method and basis set combination

predicts B_e constants that are closest to B_0 ones, even if the reason is only error compensation. Such benchmark calculations allow us faster and/or more straightforward assignments of the microwave spectra of similar molecules. In the case of *anti*-2A3MT, the MP2/6-31G(d,p) level of theory predicted the *A* rotational constant almost perfectly while *B* and *C* were also less than 1 MHz off. This level of theory has also stood out in many of our previous works where similar benchmark calculations were performed, especially for molecules containing aromatic rings such as 2-ethylfuran,[85] coumarin,[87] and *o*-methylanisole.[88] We note that the MP2/6-31G(d,p) level predicts a planar structure for *anti*-2A3MT, in contrast to some other MP2 calculations.

A similarly accurate prediction of all three rotational constants is only achieved at the two B3LYP-D3BJ/6-311+(+)G(2d,2p) levels of theory. Overall most employed levels predict the rotational constants sufficiently close to the experimental values for assignment purposes. Only a small number of them deviate by more than 10 MHz. Notably large deviations only occur for individual method/basis set combinations without any apparent trends, showing that none of the tested levels are categorically unsuitable for 2A3MT. Resort to more accurate quantum chemical calculations is not attempted, since the present study mainly focus on the effects of internal rotation arising from two inequivalent methyl rotors, using quantum chemical calculations as a supporting tool, rather than structure determination. In this sense, our benchmark only includes cost-efficient calculations allowing rapid access to rotational constants for an assignment guidance of the microwave spectrum.

The barriers to internal rotation of the acetyl methyl and the ring methyl group deduced from the *XIAM* fit are 306.184(46) cm^{-1} and 321.813(64) cm^{-1}, respectively. Compared to the predicted values, previous studies reported that though the order of magnitude is often correct,[49,65,79] MP2 calculations tend to overestimate while the B3LYP-D3(BJ) ones almost always underestimate the barrier height, which is also true for *anti*-2A3MT (see Table 2 and Table S-3 for example). No method/basis set combination manages to calculate well both the acetyl methyl and ring methyl torsional barriers at the same time, given that even small differences of the V_3 value can lead to significant changes in the torsional fine structure.

Microwave spectroscopic studies on methyl torsions in thiophene derivatives are still scarce. To the best of our knowledge, investigations on only three molecules other than 2A3MT, i.e. 2-methylthiophene (molecule (**1**) in Figure 9),[89] 2,5-dimethylthiophene (**2**),[49] and 3-methylthiophene (**3**),[90] report on the internal rotation of a methyl group attached to the thiophene ring. In all three molecules, no further substituent is in close proximity of the methyl rotor, and the barrier hindering the methyl torsion ranges from 194.1 cm^{-1} in 2-methylthiophene (**1**)[89] to 258.8 cm^{-1} in 3-methylthiophene (**3**).[90] Compared to the value of 321.8 cm^{-1} found for the ring methyl group of *anti*-2A3MT we found a significant increase due to sterical hindrance caused by the neighboring acetyl substituent.

For the acetyl methyl group, Andresen et al. introduced a classification system linking the torsional barrier with the molecular structure at the other side of the carbonyl bond.[79,91-93] This categorization clearly illustrates that electronic effects influence torsional behavior, although to understand the exact nature of this interaction more data points are necessary. To shed some lights in these interactions and with the aim of establishing a distinct “thiophene” class, further thiophene derivatives containing an acetyl substituent will be the subject of our future investigations. The two isomers of 2A3MT, 2-acetyl-4-methylthiophene (2A4MT) and 2-acetyl-5-methylthiophene (2A5MT), are currently under study to explore the influence of the substitution position of the ring methyl rotor on the torsional barriers of both methyl groups. As no steric hindrance between the acetyl methyl and the ring methyl groups is present in both 2A4MT and 2A5MT, and the internal rotors can only interact via electronic effects transferred through the *π*-conjugated system, comparison with the torsional barriers observed for 2A3MT is of special interest.

It will be also interesting to study 3-acetylthiophene and its two-top derivatives to investigate the influence of the position of the acetyl group attached to the thiophene ring. On a longer term, three or four-top derivatives of acetylthiophene will be important in order to understand more thoroughly multiple methyl rotor systems connected through a *π*-conjugation. To the best of our knowledge, only three molecules fall in this category, 1,2,5-trimethylpyrrole,[38] 2,3,4,5-tetramethylthiophene,[38] and 2,6-dimethylanisole,[94] all of which are on-going studies.

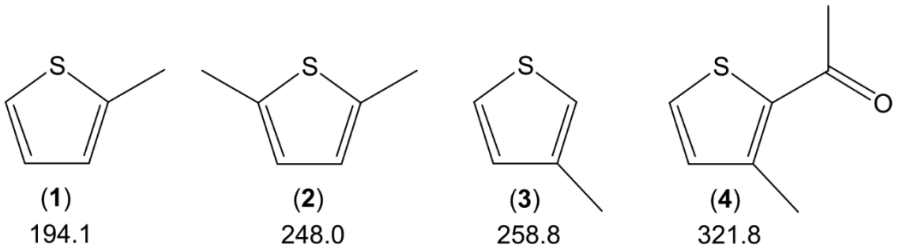

Figure 9: Torsional barriers of the ring methyl group given in cm^{-1} of (**1**) 2-methylthiophene,[89] (**2**) 2,5-dimethylthiophene,[49] (**3**) 3-methylthiophene,[90] and (**4**) *anti*-2-acetyl-3-methylthiophene (this work).

5. Conclusion

The *anti*-conformer of 2A3MT was assigned under molecular jet conditions using Fourier transform microwave spectroscopy with support from quantum chemical calculations. The two non-equivalent internal rotations of the acetyl methyl and the ring methyl groups caused splittings of all rotational transitions into five torsional species. The barriers hindering the methyl torsions were determined to be 306.184(46) cm^{-1} and 321.813(64) cm^{-1}, respectively. A comparison to the values observed for the ring methyl rotor in 2-methylthiophene, 3-methylthiophene, and 2,5-dimethylthiophene clearly implies the influence of steric effects. The experimentally determined internal defect suggests that the heavy-atom structure of the molecule is entirely planar, though several MP2 optimizations predict the acetyl group to be tilted out of the thiophene plane.

Experimental Section

A scan from 9.0 to 15.8 GHz was recorded with a molecular jet Fourier-transform microwave spectrometer operating in the frequency range from 2.0 to 26.5 GHz[94] as a series of overlapping spectra with a step width of 250 kHz. For each measurement 50 free-induction decays were co-added. 2A3MT was purchased from Sigma-Aldrich, Schnelldorf, Germany, with a stated purity of 98 % and used without any further purification. The substance was put on a 5 cm piece of pipe cleaner and placed upstream the nozzle with a backing pressure of about 2 bar helium as the carrier gas. All lines of the scan were subsequently remeasured at a higher resolution with an experimental accuracy of 2 kHz[95] in order to resolve the torsional splittings caused by the two methyl tops.

Acknowledgments

We thank Marc Kreutzer for his contribution within a student research project. Simulations were performed with computing resources granted by the RWTH Aachen University under project rwth0369. This work was supported by the Agence Nationale de la Recherche ANR (project ID ANR-18-CE29-0011).

References

[1] H.V.L. Nguyen, I. Kleiner in *Theoretical and computational chemistry*, (Eds. I. Gulaczyk, B. Tylkowski), De Gruyter, Berlin/Boston, **2021**, pp. 41-78.

[2] A.C. Legon, *Chem. Rev.* **1980**, *80*, 231-362.

[3] H.V.L. Nguyen, I. Gulaczyk, M. Kręglewski, I. Kleiner, *Coord. Chem. Rev.* **2021**, *436*, 213797.

[4] W. Gordy, R.L. Cook, Microwave molecular spectra, Vol. 18, 3rd Ed., Wiley, New York, **1984**.

[5] G.A. Cooper, C. Medcraft, E. Gougoula, N.R. Walker, *Phys. Chem. Chem. Phys.* **2019**, *21*, 9495-9503.

[6] A. Maris, L.B. Favero, A. Vigorito, C. Calabrese, L. Evangelisti, S. Melandri, *J. Mol. Struct.* **2020**, *1205*, 127643.

[7] W. Cheng, Y. Zheng, G. Feng, J.-U. Grabow, Q. Gou, *Spectrochim. Acta A* 2020, 239, 118434.

[8] M.K. Jahn, D.A. Obenchain, K.P. Rajappan Nair, J.-U. Grabow, N. Vogt, J. Demaison, P.D. Godfrey, D. McNaughton, *Phys. Chem. Chem. Phys.* **2020**, *22*, 5170-5177.

[9] V.L. Orr, Y. Ichikawa, A.R. Patel, S.M. Kougias, K. Kobayashi, J.F. Stanton, B.J. Esselman, R.C. Woods, R.J. McMahon, *J. Chem. Phys.* **2021**, *154*, 244310.

[10] J. Demaison, N. Vogt, *Accurate structure determination of free molecules;* Springer **2020**.

[11] M. Sanz-Novo, I.León, E.R. Alonso, L. Kolesniková, J.L. Alonso, *ApJ* **2021** *915,* 76.

[12] K.L.K. Lee, P.B. Changala, R.A. Loomis, A.M. Burkhardt, C. Xue, M.A. Cordiner, S.B. Charnley, M.C. McCarthy, B.A. McGuire, *ApJL* **2021**, *910,* L2.

[13] J. Cernicharo, C. Cabezas, Y. Endo, M. Agúndez, B. Tercero, J.R. Pardo, N. Marcelino, P. de Vicente, *A&A* **2021***, 650*, L14.

[14] I. León, E.R. Alonso, S. Mata, C. Cabezas, J.L. Alonso*, Angew. Chem. Int. Ed.* **2019**, *57*, 16002-16007.

[15] C. Calabrese, I. Uriarte, A. Insausti, M. Vallejo-López, F.J. Basterretxea, S.A. Cochrane, B.G. Davis, F. Corzana, E.J. Cocinero, *ACS Cent. Sci.* **2020**, 6, 293–303.

[16] E.M. Neeman. T.R. Huet, *Phys. Chem. Chem. Phys.* **2021**, *23*, 2179-2185.

[17] F. Xie, X. Ng, N.A. Seifert, J. Thomas, W. Jäger, Y. Xu, *J. Chem. Phys.* **2018**, *149*, 224306.

[18] F. Xie, M. Fusè, A.S. Hazrah, W. Jäger, V. Barone, Y. Xu, *Angew. Chem. Int. Ed.* **2020**, *59*, 22427-22430.

[19] S.R. Domingos, C. Pérez, M.D. Marshall, H.O. Leung, M. Schnell, *Chem. Sci.* **2020**, *11*, 10863-10870.

[20] D. Loru, A.L. Steber, P. Pinacho, S. Gruet, B. Temelso, A.M. Rijs, C. Pérez, M. Schnell, *Phys. Chem. Chem. Phys.* **2021**, *23*, 9721-9732.

[21] M. Chrayteh, T.R. Huet, P. Dréan, *J. Chem. Phys.* **2020**, *153*, 104304.

[22] W.G.D.P. Silva, J. van Wijngaarden, *J. Chem. Phys*. **2021**, *155*, 034305.

[23] C. Calabrese, B. Temelso, I. Usabiaga, N.A. Seifert, F.J. Basterretxea, G. Prampolini, G.C. Shields, B.H. Pate, L. Evangelisti, E.J. Cocinero, *Angew. Chem. Int. Ed.* **2021**, *60*, 16894-16899.

[24] Y. Jin, R.T. Saragi, M. Juanes, G. Feng, A. Lesarri, *Phys. Chem. Chem. Phys.* **2021**, *23*, 10799-10806

[25] S. Blanco, M.E. Sanz, A. Lesarri, J.C. López, J.L. Alonso, *Chem. Phys. Lett.* **2004**, *397*, 379-381.

[26] D.A. Obenchain, P. Pinacho, S. Zinn, M. Schnell, *J. Mol. Struct.* **2020**, *1213*, 128109.

[27] C.G. Weslley, G.D.P. Silva, J. van Wijngaarden, *J. Mol. Spectrosc.* **2021**, *377*, 111444.

[28] T. Ogata, K. Kunio, *Bull. Chem. Soc. Jpn.* **1971**, *44*, 2344-2346.

[29] V. Ilyushin, R. Rizzato, L. Evangelisti, G. Feng, A. Maris, S. Melandri, W. Caminati, *J. Mol. Spectr.* **2011**, *267*, 186-190.

[30] D.S. Wilcox, A.J. Shirar, O.L. Williams, B.C. Dian, *Chem. Phys. Lett.* **2011**, *508*, 10-16.

[31] S. Herbers, P. Kraus, J.-U. Grabow, *J. Chem. Phys.* **2019**, *14*, 144308.

[32] N. Ohashi, J.T. Hougen, R. D. Suenram, F.J. Lovas, Y. Kawashima, M. Fujitake, J. Pyka, *J. Mol. Spectrosc.* **2004**, *227*, 28–42.

[33] D.F. Plusquellic, I. Kleiner, J. Demaison, R.D. Suenram, R.J. Lavrich, F.J. Lovas, G.T. Fraser, V.V. Ilyushin *J. Chem. Phys.* **2006**, *125*, 104312.

[34] E.G. Schnitzler, B.L.M. Zenchyzen, W. Jäger *ApJ,* **2015**, *805,* 141.

[35] I. Merke, A. Lüchow, W. Stahl, *J. Mol. Struct.* **2006**, *780-781*, 295-299.

[36] M. Schnell, J.T. Hougen, J.-U. Grabow, *J. Mol. Spectrosc*. **2008**, *251*, 38-55.

[37] M. Fujitake, Y. Kubota, N. Ohashi, *J. Mol. Spectrosc.* **2006**, *236*, 97-109.

[38] V. Van, *Structures and Internal Dynamics of Cyclic Molecules Studied by Microwave Spectrsocopy and Quantum Chemistry*, RWTH Aachen University **2017**.

[39] H. Dreizler, *Z. Naturforsch.* **1961**, *16a*, 1354-1367.

[40] L. Ferres, K.-N. Truong, W. Stahl, H.V.L. Nguyen, *ChemPhysChem* **2018**, *19*, 1781-1788.

[41] L. Ferres, J. Cheung, W. Stahl, H.V.L. Nguyen, *J. Phys. Chem. A.* **2019**, *123*, 3497-3503.

[42] L. Ferres, W. Stahl, H.V.L. Nguyen, *J. Chem. Phys.* **2019**, *151*, 104310.

[43] M. Tudorie, I. Kleiner, M. Jahn, J.-U. Grabow, M. Goubert, O. Pirali, *J. Phys. Chem. A.* **2013**, *117*, 13636-13647.

[44] H.D. Rudolph, K. Walzer, I. Kreutzik, *J. Mol. Spectrosc*. **1973**, *47*, 314-339.

[45] C. Thomsen, H. Dreizler, *Z. Naturforsch*. **2001**, *56 a*, 635-640.

[46] S. Khemissi, H.V.L. Nguyen, *ChemPhysChem* **2020**, *21*, 1682-1687.

[47] J. Mélan, S. Khemissi, H.V.L. Nguyen, *Spectrochim. Acta A* **2021**, *253*, 119564.

[48] S. Herbers, S.M. Fritz, P. Mishra, H.V.L. Nguyen, T.S. Zwier, *J. Chem. Phys.* **2020**, *152*, 074301.

[49] V. Van; W. Stahl, H.V.L. Nguyen*, Phys. Chem. Chem. Phys.* **2015**, *17*, 32111-32114.

[50] V. Van, J. Bruckhuisen, W. Stahl, V. Ilyushin, H.V.L. Nguyen, *J. Mol. Spectrosc.* **2018**, *343*, 121-125.

[51] T. Nguyen, W. Stahl, H.V.L. Nguyen, I. Kleiner, *J. Chem. Phys.* **2021**, *154*, 204304.

[52] V. Van; W. Stahl, H.V.L. Nguyen, *ChemPhysChem*. **2016**, *17*, 3223–3228.

[53] V. Van, T. Nguyen, W. Stahl, H.V.L. Nguyen, I. Kleiner, *J. Mol. Struct.* **2020**, *1207*, 127787.

[54] B. Bak, D. Christensen, L. Hansen-Nygaard, J. Rastrup-Andersen, *J. Mol. Spectrosc*. **1961**, *7*, 58-63.

[55] C. Dindić, A. Lüchow, N. Vogt, J. Demaison, H.V.L. Nguyen *J. Phys. Chem. A.* **2021**, *125*, 4986-4997.

[56] R. Hakiri, N. Derbel, W. C. Bailey, H.V.L. Nguyen, H. Mouhib, *Mol. Phys.* **2020**, *118*, e1728406.

[57] Gaussian 16, Revision B.01, M.J. Frisch, G.W. Trucks, H.B. Schlegel, G.E. Scuseria, M.A. Robb, J.R. Cheeseman, G. Scalmani, V. Barone, G.A. Petersson, H. Nakatsuji, X. Li, M. Caricato, A.V. Marenich, J. Bloino, B.G. Janesko, R. Gomperts, B. Mennucci, H.P. Hratchian, J.V. Ortiz, A.F. Izmaylov, J.L. Sonnenberg, D. Williams-Young, F. Ding, F. Lipparini, F. Egidi, J. Goings, B. Peng, A. Petrone, T. Henderson, D. Ranasinghe, V. G. Zakrzewski, J. Gao, N. Rega, G. Zheng, W. Liang, M. Hada, M. Ehara, K. Toyota, R. Fukuda, J. Hasegawa, M. Ishida, T. Nakajima, Y. Honda, O. Kitao, H. Nakai, T. Vreven, K. Throssell, J.A. Montgomery, Jr., J.E. Peralta, F. Ogliaro, M.J. Bearpark, J.J. Heyd, E.N. Brothers, K.N. Kudin, V.N. Staroverov, T.A. Keith, R. Kobayashi, J. Normand, K. Raghavachari, A. P. Rendell, J.C. Burant, S.S. Iyengar, J. Tomasi, M. Cossi, J.M. Millam, M. Klene, C. Adamo, R. Cammi, J.W. Ochterski, R.L. Martin, K. Morokuma, O. Farkas, J.B. Foresman, and D.J. Fox, Gaussian, Inc., Wallingford CT, **2016**.

[58] E.G. Schnitzler, N.A. Seifert, S. Ghosh, J. Thomas, Y. Xu, W. Jager, *Phys. Chem. Chem. Phys.* **2017**, *19*, 4440-4446.

[59] M.E. Sanz, S. Blanco, J.C. Lopez, J.L. Alonso*, Angew. Chem. Int. Ed.* **2008,** *47*, 6216-6220.

[60] P. Ottaviani, B. Velino, W. Caminati, *Chem. Phys. Lett.* **2006**, *428*, 236-240.

[61] J.-R.A. Moreno, D. Petitprez, T.R. Huet, *Chem. Phys. Lett.* **2006**, *419*, 411-416.

[62] V. Van, W. Stahl, M. Schwell, H.V.L. Nguyen, *J. Mol. Struct.* **2018**, *1156*, 348-352.

[63] R. Kannengießer, W. Stahl, H.V.L. Nguyen, *J. Phys. Chem. A* **2016**, *120*, 5979-5984.

[64] V. Van, C. Dindić, H.V.L. Nguyen, W. Stahl, *ChemPhysChem* **2015**, *16*, 291-294.

[65] C. Dindić, W. Stahl, H.V.L. Nguyen*, Phys. Chem. Chem. Phys.* **2020**, *22*, 19704-19712.

[66] D.S. Tikhonov, D.I. Sharapa, A.A. Otlyotov, P.M. Solyankin, A.N. Rykov, A.P. Shurinov, O.E. Grikina, L.S. Khakin, *J. Phys. Chem. A.* **2018**, *122*, 1691–1701.

[67] C. Møller, M.S. Plesset, *Phys. Rev.* **1934**, *46*, 618-622.

[68] A.D. Becke, *J. Chem. Phys.* **1993**, *98*, 5648−5652.

[69] C. Lee, W. Yang, R.G. Paar, *Phys. Rev. B* **1988**, *37*, 785−789.

[70] G.E. Scuseria, A.C. Scheiner, T.J. Lee, J.E. Rice, H.F. Schaefer III, *J. Chem. Phys.* **1987**, *86*, 2881-2890.

[71] Y. Zhao, D.G. Truhlar, *Theor. Chem. Acc.* **2008**, *120*, 215-241.

[72] J.-D. Chai, M. Head-Gordon, *Phys. Chem. Chem. Phys.* **2008**, *10*, 6615-6620.

[73] S. Grimme, S. Ehrlich, L. Goerigk, *J. Comput. Chem.* **2011**, *32*, 1456-1465.

[74] S. Grimme, J. Antony, S. Ehrlich, H. Krieg, *J. Chem. Phys.* **2010**, *132*, 154104.

[75] T. Yanai, D.P. Tew, N.C. Handy, *Chem. Phys. Lett.* **2004**, *393*, 51-57.

[76] M.J. Frisch, J.A. Pople, J.S. Binkley, *J. Chem. Phys.* **1984**, *80*, 3265-3269.

[77] T.H. Dunning Jr., *J. Chem. Phys.* **1989**, *90*, 1007-1023.

[78] R.A. Kendall, T.H. Dunning Jr., R.J. Harrison, *J. Chem. Phys.* **1992**, *96*, 6796-6806.

[79] M. Andresen, I. Kleiner, M. Schwell, W. Stahl, H.V.L. Nguyen, *J. Phys. Chem. A.* **2020**, *124*, 1353–1361.

[80] K.L.K. Lee, M. McCarthy, *J. Phys. Chem. A* **2020**, *124*, 898-910.

[81] H. Hartwig and H. Dreizler, *Z.Naturforsch.* **1996**, *51a*, 923-932.

[82] S. Herbers, S.M. Fritz, P. Mishra, H.V.L. Nguyen, T.S. Zwier, *J. Chem. Phys*., **2020**, *152*, 074301.

[83] V. Typke, *Z. Naturforsch.* **1971**, *26a*, 175-177.

[84] E.D. Glendening, C.R. Landis, F. Weinhold, *WIREs Comput. Mol. Sci.* **2012**, *2*, 1-42.

[85] H.V.L. Nguyen, *J. Mol. Struct.* **2020**, *1208*, 127909.

[86] N. Hansen, F. Temps, H. Mäder, N.W. Larsen, *Phys. Chem. Chem. Phys*. **1999**, *1*, 3219-3233.

[87] H.V.L. Nguyen, J.-U. Grabow, *ChemPhysChem* **2020**, *21*, 1243-1248.

[88] L. Ferres, H. Mouhib, W. Stahl, H.V.L. Nguyen, *ChemPhysChem* **2017**, *18*, 1855-1859.

[89] N.M. Pozdeev, L.N. Gunderova, A.A. Shapkin, *Opt. Spectrosc.* **1970**, *28*, 254.

[90] T. Ogata, K. Kozima, *J. Mol. Spectrosc*., **1972**, *42*, 38-46.

[91] M. Andresen, I. Kleiner, M. Schwell, W. Stahl, H.V.L. Nguyen, *J. Phys. Chem. A.* **2018**, *122*, 7071–7078.

[92] M. Andresen, I. Kleiner, M. Schwell, W. Stahl, H.V.L. Nguyen, *ChemPhysChem* **2019**, *20*, 2063–2073.

[93] M. Andresen, M. Schöngen, I. Kleiner, M. Schwell, W. Stahl, H.V.L. Nguyen, *ChemPhysChem* **2020**, *21*, 2206–2216.

[94] L. Ferres, *Quantum Chemical and Microwave Spectroscopic Investigations on Phenyl Ring Containing Molecules*, RWTH Aachen University **2019**.

[94] J.-U. Grabow, W. Stahl, H. Dreizler, *Rev. Sci. Instrum*. **1996**, *67*, 4072–4084.

[95] J.-U. Grabow, W. Stahl, *Z. Naturforsch*. **1990**, *45a*, 1043–1044.